Hsa-miR-375 Is Differentially Expressed During Breast Lobular Neoplasia And Promotes Loss Of Mammary Acinar Polarity

Running Title: Hsa-mir-375 expression during lobular neoplasia progression

Orsi Giricz[1], Paul A. Reynolds[5], Andrew Ramnauth[2], Christina Liu[2], Tao Wang[2], Lesley Stead[5], Geoffrey Childs[3], Thomas Rohan[2], Nella Shapiro[4], Susan Fineberg[3,4], Paraic A Kenny[1], Olivier Loudig[2, 3].

Departments of Developmental and Molecular Biology[1], Epidemiology and Population Health[2], and Pathology[3], Albert Einstein College of Medicine, Bronx, NY, USA. [4]Montefiore Medical Center, Bronx, NY, USA. [5]Medical and Biological Sciences Building, School of Medicine, University of St Andrews, St Andrews, UK.

For correspondence:
paraic.kenny@einstein.yu.edu; olivier.loudig@einstein.yu.edu

Original publication: The work presented in this manuscript contains original unpublished work and is not being submitted for publication elsewhere at the same time.

Conflict of Interest Statement: The authors have no conflicts of interest to disclose.

Word Count: 3,999

GEO data Submission: microRNA profiling raw data and normalized data have been submitted and posted onto the GEO website. Please find the data at the link below:
http://www.ncbi.nlm.nih.gov/geo/query/acc.cgi?acc=GSE28514

This is an Accepted Article that has been peer-reviewed and approved for publication in *The Journal of Pathology*, but has yet to undergo copy-editing and proof correction. Please cite this article as an "Accepted Article"; DOI: 10.1002/path.2978

ABSTRACT

Invasive lobular carcinoma (ILC) of the breast, characterized by loss of E-cadherin expression, accounts for 5-15% of invasive breast cancers and it is believed to arise via a linear histological progression. Genomic studies have identified a clonal relationship between ILC and concurrent lobular carcinoma *in situ* (LCIS) lesions, suggesting that LCIS may be a precursor lesion. It has been shown that an LCIS diagnosis confers a 15-20% risk of progression to ILC over a lifetime. Currently no molecular test or markers can identify LCIS lesions likely to progress to ILC. Since microRNA (miRNA) expression changes have been detected in a number of other cancer types, we explored whether their dysregulation might be detected during progression from LCIS to ILC. Using the Illumina miRNA profiling platform, designed for simultaneous analysis of 470 mature miRNAs, we analyzed the profiles of archived normal breast epithelium, LCIS lesions found alone, LCIS lesions concurrent with ILC, and the concurrent ILCs, as a model of linear histological progression toward ILC. We identified two sets of differentially expressed miRNAs, the first set highly expressed in normal epithelium, including hsa-miR-224, -139, -10b, -450, 140 and -365 and the second set upregulated during lobular neoplasia progression, including hsa-miR-375, -203, -425-5p, -183, -565 and -182. Using quantitative RT-PCR, we validated a trend of increasing expression for hsa-mir-375, hsa-mir-182, and hsa-mir-183 correlating with ILC progression. As we detected increased expression of hsa-miR-375 in LCIS lesions synchronous with ILC, we sought to determine whether hsa-mir-375 might induce phenotypes reminiscent of lobular neoplasia by expressing it in the MCF10A 3D culture model of mammary acinar morphogenesis. Increased expression of hsa-miR-375 resulted in loss of cellular organization and acquisition of a hyperplastic phenotype. These data suggest that dysregulated miRNA expression contributes to lobular neoplastic progression.

Keywords: lobular carcinoma, microRNA, acinar morphogenesis

INTRODUCTION

Invasive lobular carcinoma (ILC) comprises approximately 5-15% of invasive breast cancer cases and various studies report five-year average survival rates between 68-87% [1] Stage at diagnosis has a pronounced effect, with a five-year disease-specific survival rate of 98% in patients with T1N0 ILC and 72% in patients with T3N1 disease [2]. A spectrum of precursor lesions, termed lobular intra-epithelial neoplasia, has been defined, and they include atypical lobular hyperplasia and lobular carcinoma *in situ* (LCIS), characterized by several variants [3]. Genomic studies using archived specimens of LCIS found synchronously with ILC have shown a high degree of homology in chromosomal imbalances between these two lesions [4,5,6], indicating a clonal relationship between them, and further suggesting that LCIS may act as a precursor lesion of ILC. Molecular analyses have also revealed identical E-cadherin mutations in synchronous LCIS and ILC lesions [7].

The recognized variants of LCIS include classical LCIS, pleiomorphic LCIS, and LCIS with comedo necrosis [8,9,10]. While classical and pleiomorphic LCIS are E-cadherin negative, they exhibit important differences in their immunophenotypes. Classical LCIS has a low proliferative rate (low Ki67), is typically oestrogen receptor positive (and progesterone receptor positive) and rarely shows HER2 overexpression or p53 mutation. Pleiomorphic LCIS typically has a higher proliferative rate (high ki67), may be hormone receptor negative and may show p53 mutation and/or HER2 overexpression [8,10,11]. LCIS is frequently multifocal and bilateral and a biopsy finding of LCIS is associated with an increased risk of invasive breast cancer of 10-20% over 15 to 20 years [12,13].

The pathogenesis of LCIS and ILC and the factors promoting progression along this lineage remain poorly understood and while the majority of LCIS lesions do not progress to ILC, no biomarkers are available to distinguish high- and low-risk lesions. We propose that comparing LCIS lesions found synchronously with ILC with LCIS lesions from patients without concurrent ILC, will help identify mechanism(s) and biomarkers associated with progression of

LCIS to ILC.

Recent studies have shown that the genes coding for microRNAs (miRNAs) are frequently located in cancer-associated genomic regions or in fragile sites and their aberrant expression might contribute to the development and progression of cancer [14,15]. MiRNAs are non-coding RNA molecules, 18 to 24 nucleotides in length, that regulate the translation and degradation of target mRNAs through base pairing in the 3' untranslated regions (UTRs). MiRNA genes can be found either as individual or clustered genes in the genome or as embedded sequences within functional genes, in introns or in exons [16]. To date more than 1,000 human miRNAs have been identified, and studies have shown that miRNAs can bind multiple mRNA transcripts and regulate several pathways involving development, cellular proliferation and differentiation, adhesion, migration, invasion, apoptosis and many other biological processes relevant to cancer development and progression [17]. MiRNA expression studies in breast cancer have demonstrated that miRNAs can act as tumour suppressors or as oncogenes [18,19].

In this study, we have examined the potential role of miRNAs in the progression from normal mammary tissue, through LCIS to ILC. We performed high-throughput miRNA profiling on normal, LCIS and ILC specimens to determine whether miRNAs may be dysregulated during neoplastic progression of this disease and specifically analyzed the expression of hsa-miR-375 and its contribution to mammary epithelial architecture.

MATERIALS AND METHODS

Human specimens. Thirty-one archived specimens were obtained from Montefiore Medical Center (MMC), Bronx, NY, after approval of the study by the Institutional Review Board. These specimens included two normal breast specimens (frozen and matched 1 month-old FFPE), 5 normal lobular breast tissues, 7 specimens containing LCIS lesions alone, 8 containing LCIS lesions synchronous with ILC, 8 matched specimens containing ILC lesions, and 1 ILC found alone. The ILC specimens were all confirmed by negative E-cadherin staining. One normal pancreas was used for *in situ* hybridization analysis.

Histology and Immunohistochemistry. Twelve sections were obtained from each archived breast specimen (1-3 years-old), the first and last being Haematoxylin and Eosin (H&E) stained slides, and 10 intermediate 10 μm unstained sections. Lesions were identified on H&E slides and used as guides for macrodissection on unstained slides. E-cadherin immunohistochemistry was performed using the Zymed® antibody clone 4A2C7, following manufacturer's instructions, at the MMC pathology laboratory.

RNA extraction and quantification. RNA from the frozen sample was extracted using TRIzol (Invitrogen). RNA from archived breast specimens was extracted using a previously described method [20]. For qRT-PCR all RNA samples were extracted using the High Pure RNA paraffin kit (Roche Applied Science), following manufacturer's instructions. Total RNA was quantified on a Nanodrop ND-2000 spectrophotometer and analyzed on a Bioanalyzer mRNA Nanochip (Agilent).

MiRNA expression profiling. These experiments were performed on a Sentrix array matrix (96 beadarrays) using the Illumina miRNA profiling platform for simultaneous analysis of 735 probes (470 mature miRNAs), using 200ng of total RNA accordingly to manufacturer's instructions [21]. Arrays were scanned on a beadarray reader (Illumina) and raw data were obtained from Beadstudio (3.3).

Reverse transcription and PCR quantifications. Taqman® miRNA primers, miRNA reverse

transcription kit, and universal PCR master mix, No AmpErase® UNG (Applied Biosystems (AB), USA) were used for these experiments. Individual RT reactions using 10ng of total RNA were assembled in PCR tubes following the manufacturer's instructions (AB). PCR quantifications were monitored on a StepOnePlus instrument (AB) and comparative thresholds were determined by averaging results of triplicate reactions. Both RNU44 and RNU6B were used as endogenous controls for data normalization. The ΔC_t of each miRNA, was determined by subtracting the mean C_t value of RNU44 and RNU6B from the C_t value of each miRNA. The $\Delta\Delta C_t$, for each miRNA in each sample, was determined by subtracting the ΔC_t of the control samples (mean of ΔC_t of 5 normal samples) from the ΔC_t of the samples of interest. The fold change differences were calculated using the $2^{(\Delta\Delta Ct)}$ formula.

***In Situ* Hybridization (ISH)**. These experiments were performed following the procedure described by Jorgensen *et. al.* [22], using a 20 minute Proteinase K treatment of the sections and Exiqon double-DIG miRCURYLNA probes including a Scramble-miR, hsa-miR375 at 40nM, anddouble-DIG miRCURYLNA U6 probe at 20nM. Incubations were performed in array chambers in a water bath.

Cell Lines and Maintenance. Non-tumourigenic breast epithelial MCF-10A cells were cultured in DMEM/F12 (Cellgro), supplemented with 5% horse serum (Invitrogen), hydrocortisone (0.5µg/ml), mouse epidermal growth factor (EGF; 20ng/ml), insulin (10µg/ml), cholera toxin (100ng/ml, SIGMA, Saint Louis, MO) at 37°C in a humidified incubator (5% CO_2). Human primary miR-375 (pri-miR-375) and a non-silencing control miRNA were stably and separately expressed in MCF10A cells by lentiviral gene transfer using pLemiR expression system (ThermoFisher). The pLemiR constructs expressed TurboRed fluorescent protein (Evrogen) and a puromycin resistance selectable marker. Stable populations were obtained by selection with puromycin (2.5g/ml, MP Biomedicals), and detection of TurboRFP.

Immunofluorescence staining and confocal microscopy of MCF-10A Acini. Trypsinized

single cell suspensions of MCF10A cells were seeded on top of growth factor-reduced Matrigel (BD sciences) at 2% (without EGF) with growth medium (replaced every 3-4 days), at a density of 2,900 per cm^2 [24]. Immunostaining was carried out as described by Debnath *et al.* [23]. In short, the acini were fixed in Matrigel with 4% Paraformaldehyde (20min at room temperature (RT)) and permeabilized with Triton X-100 (0.5% in PBS, 10min at 4°C). After three washes with glycine (100mM in PBS), primary blocking was carried out for 2h at RT in PBS containing BSA ,0.1%; Triton X-100, 0.2%; Tween-20, 0.05% and goat serum, 10%). A secondary block was carried out for 45 minutes at RT using the same blocking buffer with the addition of goat anti-mouse $F(ab')_2$ fragment (20µg/ml, Jackson ImmunoResearch). The samples were incubated with 1:100 anti-CD49f (α6-integrin from BD Biosciences) in full secondary block buffer overnight at 4°C. The AlexaFluor conjugated secondary antibody (Invitrogen) was used at 1:200 dilution in full primary block buffer for 1h at RT. The nuclei were counterstained with Hoechst 33342 (1μM) for 15 minutes at RT. Confocal analyses were performed with a Leica TCS SP2 AOBS confocal microscope (Mannheim, Germany) with a 25X oil immersion objective.

Data analysis. Raw data files were imported into Partek Genomics Suite (6.5). The Partek Batch Remover tool (an ANOVA-based method) was used to control for batch effect, data were quantile normalized, and analyzed using ANOVA to identify miRNAs differentially expressed between neoplastic and normal specimens. For qRT-PCR experiments, p-values testing for trend between the four groups were obtained by linear regression and are presented as inset Box plots. By including an ordered variable, based on the cancer groups (Group#1: normal, Group#2: LCIS alone, Group#3: LCIS synchronous with ILC, Group#4: the synchronous ILCs) in the model as a continuous variable, the test performed on the coefficient is equivalent to a test for a linear increase of hsa-miR-375, -182, -183 expression (Δc_t values) across the four groups [24,25].

RESULTS

Histological presentation of lobular neoplasia. Figure 1 displays one specimen with normal lobular epithelium, one classical lobular carcinoma *in situ* (LCIS) found alone without presence of an invasive breast cancer (LCISa); one pleiomorphic LCIS with necrosis found synchronously with invasive lobular carcinoma (ILC) (LCISs), and the synchronous ILC (ILCs) from the same patient. As loss of E-cadherin expression is a defining feature of lobular neoplasia [11], its immunodetection was used to distinguish normal lobules from neoplastic counterparts (Fig. 1, left column of panels). Regions of interest were identified from H&E-stained slides (Fig. 1, centre column of panels) and carefully dissected on unstained sections (Fig. 1, right column of panels).

MiRNA expression profiling of lobular neoplasia. To determine the distribution of miRNAs in normal breast epithelial cells and at successive stages of lobular neoplastic progression, we performed high-throughput profiling of 735 probes (corresponding to 470 miRNAs) with RNA extracted from the specimens displayed in Figure 1.

To evaluate the accuracy of miRNA profiling experiments with formalin-fixed paraffin-embedded (FFPE) RNA, we compared miRNA expression results between matched frozen and 1 month-old FFPE normal breast tissues. Duplicates for the frozen RNA samples ($r^2 > 0.98$) and FFPE RNA ($r^2 > 0.97$) were highly concordant with each other ($r^2 > 0.90$) (data not shown) and clustered together during the analysis (Fig. 2) Similarly, miRNA profiles of archived normal lobular epithelium, LCIS and ILC samples provided highly concordant duplicates ($r^2 > 0.979$ in all cases), which clustered together during the analysis. Using a cutoff of $p<0.02$, the ANOVA analysis identified 85 miRNAs differentially expressed between normal and neoplastic samples. These miRNAs were used for hierarchical clustering of the samples (Euclidean method, Fig. 2). Our analysis also revealed that miRNA expression profiles of LCIS and ILC samples, found synchronously in the same patient but obtained from separate archived blocks, clustered

together, suggesting a molecular relationship between LCIS and ILC [4,5].

Two groups emerged from the hierarchical clustering (Fig. 2), which included six miRNAs highly expressed in normal specimens: hsa-mir-224, hsa-mir-139, hsa-mir-10b, hsa-mir-450, hsa-mir-140 and hsa-mir-365; and six miRNAs, expressed at low levels in normal tissue but elevated in LCIS and ILC samples: hsa-mir-375, hsa-mir-182, hsa-mir-425-5p, hsa-mir-183, hsa-mir-196a, and hsa-miR-565 (Fig. 2).

Quantitative RT-PCR analyses of hsa-miR-375, -183, and -182 in archived samples. Because miRNA expression analyses revealed that hsa-mir-375 was most differentially expressed in lobular neoplasia, and because hsa-mir-182 and hsa-miR-183 belong to the same miRNA cluster and appeared co-expressed during progression of lobular neoplasia, we selected these three miRNAs for qRT-PCR studies on a larger set of clinical samples (n=28; Table 1). We used two of the profiled specimens (the LCIS synchronous with ILC, and the synchronous ILC) and 26 additional specimens. We established a baseline by measuring the expression of each miRNA in five normal lobular breast epithelium samples and determined the level of each miRNA in the neoplastic samples relative to that baseline.

QRT-PCR experiments displayed in Figure 3 demonstrate a trend of increasing expression for hsa-miR-375 ($p < 0.003$), hsa-miR-182 ($p < 0.001$), and hsa-miR-183 ($p < 0.003$) with increasing histological severity of the lesions, with the lowest expression levels in normal lobular specimens and highest expression levels in ILC specimens. Hsa-miR-182 and hsa-miR-183 displayed similar trends of increased expression, possibly related to their localization in the hsa-miR183/182/96 cluster [26].

Hsa-mir-375 expression in neoplastic cells. We selected hsa-miR-375 for further *in-situ* hybridization (ISH) validation because it displayed the highest expression levels on the Illumina miRNA beadchips and in qRT-PCR experiments, in comparison to hsa-miR-182 and hsa-miR-183. Our data shows that hsa-mir-375 displayed low expression levels in normal samples and in LCIS specimens found alone (without a synchronous ILC), while showing

increased expression levels in LCIS and ILC synchronous cases (Fig. 3, hsa-miR-375). Increased expression was observed in both histologically high-grade pleiomorphic LCIS cases (Fig. 3 hsa-miR-375, first and last bar in the LCIS synch group; LCIS synch1 and LCIS synch8 in Table 1) and the LCIS with necrosis (Fig. 3 hsa-miR-375, third bar in LCIS synch group; LCIS synch3 in Table1). Although the tissue dissection approach was designed to exclude stromal tissue, it remained possible that high levels of hsa-mir-375 may have originated from infiltrating stromal cells. Thus, we performed ISH experiments with archived specimens to localize and validate the expression of hsa-miR-375 (Fig. 4). We optimized our *in situ* detection of hsa-miR-375 on human archived pancreas, as pancreatic islets of Langerhans have been reported to express high levels of hsa-miR-375 [27,28]. QRT-PCR with RNA extracted from a 1 year-old FFPE pancreas revealed that hsa-miR-375 expression was 1,078 fold higher than in normal breast epithelium (data not shown). We used H&E staining to distinguish the endocrine islets of Langerhans (Fig. 4a, see arrows, light staining) from the exocrine pancreas (darker staining). ISH detection of hsa-miR-375 revealed robust expression in the islets of Langerhans (Fig. 4b, hsa-miR-375, purple stain) compared to the surrounding exocrine tissue. No staining was observed with the negative control scrambled probe (Fig. 4b, scrambled). The expression pattern of hsa-mir-375 in the pancreas validated our detection assay. We applied to same ISH procedure to archived breast specimens (Fig. 4c). The scrambled miRNA probe resulted in no staining (Fig 4c, left column) while ISH detection of hsa-mir-375 revealed weak expression in normal breast epithelium and LCIS lesions found alone, but the highest expression levels within LCIS and ILC lesions found synchronously. These data support the differential expression of hsa-mir-375 observed by high-throughput miRNA profiling (Fig. 2), and qRT-PCR experiments (Fig. 3), and confirm that hsa-mir-375 is primarily expressed in the neoplastic cells of these specimens. Similar ISH detection data were obtained for hsa-mir-182, the second highest expressed miRNA after hsa-miR-375 (see additional Figure).

Hsa-miR-375 expression disrupts mammary acinar morphogenesis.

Analysis of miRNA expression in a larger set of clinical samples would be necessary to determine whether the expression levels of hsa-miR-375, hsa-miR-182, and hsa-miR-183 may have prognostic utility but also help identify other upregulated and downregulated miRNAs, which may correlate with lobular neoplasia progression. However, because increased expression of hsa-miR-375, in MCF7 cells, has been associated with increased proliferation [29], and its expression is found at its highest levels in LCIS synchronous with ILC (Figs 2-4), we hypothesized that increased expression of hsa-miR-375 may contribute to progression of lobular breast neoplasia. We used the MCF10A model of mammary acinar morphogenesis to test the effect of increased expression of hsa-miR-375. When this cell line is cultured within a reconstituted basement membrane (Matrigel), it forms small colonies, which, over a period of time develop the central lumen and apicobasal polarity that characterize human mammary epithelial cells *in vivo*. Experimental overexpression of various oncogenes in MCF10A cells, in 3D culture, leads to phenotypes including hyperplastic growth, failure of apoptosis, and formation of multilobular colonies [30]. To determine whether increased expression of hsa-mir-375 may affect the maintenance of correct breast tissue polarity in 3D culture, we used lentiviral expression to stably express hsa-miR-375 in MCF10A cells. QRT-PCR analysis (Fig. 5A) evaluated the levels of hsa-mir-375 in MCF10A^{ctrl} cells and MCF10A$^{hsa\text{-}miR\text{-}375}$ cells, by comparison with hsa-miR-375 expression levels in normal breast epithelium and the LCIS synchronous with ILC case that displayed the highest expression (Fig. 3, LCISsynch1). QRT-PCR results demonstrate that hsa-mir-375 is expressed at low levels in the MCF10A^{ctrl} cells and at high levels in MCF10A $^{hsa\text{-}miR\text{-}375}$ cells, comparable to the levels detected in the LCIS synchronous with ILC (Fig. 3, see hsa-miR-375 LCISsynch1).

Pools of infected cells were selected using puromycin and analysis of co-expressed RFP was performed prior to each experiment to confirm that the majority of cells in the pool had retained the lentivirus (Fig. 5b). MCF10A cells were seeded singly on top of Matrigel [23, 28] and allowed to form colonies for four weeks (Fig. 5c, left). MCF10A cells expressing hsa-mir-

375 formed larger and more misshapen colonies, and the relative difference in cross-sectional area was highly statistically significant (Fig. 5c, right). In addition, hsa-mir-375-expressing colonies cleared significantly fewer cells from the centre of the colonies compared to the vector control. We further analyzed the status of tissue polarity in these structures, using α6-integrin as a marker of basal tissue polarity. In MCF10A^{ctrl} cells, α6-integrin was localized at the basal surface of these cells, while this organization was completely disrupted in the MCF10A$^{hsa\text{-}mir\text{-}375}$ colonies. These data suggest that increasing hsa-mir-375 expression to levels found in human lobular neoplasia specimens may alter the ability of human breast epithelial cells to establish and maintain appropriate tissue organization.

DISCUSSION

We report the first study to identify a number of upregulated miRNAs during progression of lobular neoplasia. When we transduced and overexpressed hsa-mir-375, one of the miRNAs upregulated during in lobular neoplasia, in MCF10A cells in a model of human mammary acinar morphogenesis, we found that it led to the production of larger dysmorphic colonies with filled lumens, and substantial perturbations in tissue polarity; phenotypes recapitulating, at least in part, the ones observed during lobular neoplasia. This study is the first to show that ectopic expression of a single miRNA can interfere with the organization of human breast epithelial cells in a 3D context.

MiRNAs are key regulators of gene expression, and abnormal expression of these molecules has been shown to correlate with the progression of many human cancers [14]. MiRNA expression studies of human breast tumours have shown that these molecules can be utilized as prognostic markers [19,31]. Although the number of specimens analyzed here was too small to develop a prognostic signature, our study strongly indicates that miRNA expression analysis in larger cohorts may allow the development and validation of prognostic or predictive signatures in lobular neoplasia.

Our qRT-PCR analyses focused on three upregulated miRNAs, hsa-miR-182, hsa-miR-183 and hsa-miR-375, and showed that expression changes follow transition from normal, to pre-invasive, to invasive lobular carcinomas. Our results show that upregulation of hsa-miR-182 and hsa-miR183 is detected in LCIS lesions synchronous with ILC. Upregulation of both hsa-miR-182 and hsa-miR-183 has been described in breast cancer cells and recently in DCIS, when compared with normal breast epithelium, supporting the idea that these two miRNAs may play important roles in the development of breast cancer [32]. Increased expression of hsa-miR-182 in MCF-7 cells has been linked with downregulation of FOXO1, a transcription factor orchestrating genes involved in apoptotic response, cell cycle checkpoints, and cellular metabolism [33]. Using MCF-7 cells, Hannafon et al. [7], recently identified 4 additional targets

(CBX7, DOK4, NMT2 and EGR1) and their results suggest that hsa-miR-182 may also be indirectly involved in downregulation of E-cadherin expression in DCIS, an interesting finding as loss of E-cadherin is a hallmark of LCIS. Although our analysis of LCIS and the analysis of DCIS have converged on similar miRNA dysregulations, it is important to note that gene expression patterns may differ between DCIS and LCIS, as gene expression patterns differ in their respective invasive cancers, thus providing distinct gene targets involved in different pathways [32,34]. Our data shows that hsa-miR-182 and hsa-miR-183 are co-dysregulated in the same LCIS samples. These two miRNAs are clustered with hsa-miR-96 on chromosome 7q32.2, a region frequently amplified in melanoma [35]. Co-dysregulation of hsa-miR-182 and hsa-miR183 has also been described in prostate and colon cancers, but their co-expression in normal tissue has been associated with development of the inner ear, suggesting common transcriptional regulation mechanisms for these miRNAs [36,37,38]. Together, decrease of cellular adhesion (loss of E-cadherin), decrease of apoptosis, disruption of cell-cycle checkpoints, and cellular metabolism suggest that dysregulation of hsa-miR-182 and hsa-miR-183 may play important roles in breast cancer and our results suggest that these miRNAs may play important roles in the progression of pre-invasive lesions toward invasive cancers.

Strong upregulation of hsa-miR-375 in LCIS lesions synchronous with ILC and high expression in the synchronous ILC cells suggests an important role for this miRNA in the transition from pre-invasive to invasive lobular cancer cells. The dysregulated expression of hsa-miR-375 has been reported in at least five different human cancers, including gastric [39,40], head and neck [41], and liver cancers [42,43], where the expression of hsa-miR-375 is down-regulated by comparison with normal tissues; and lung [44] and breast cancers [29] where hsa-miR-375 expression is upregulated. The study of De Souza Rocha *et al.* [2], on the ER-positive (ER+) MCF-7 breast cancer cell line, has suggested that increased expression of hsa-mir-375 may play a role in the progression of ER+ breast tumors by indirectly increasing ERα expression and thus cellular proliferation, an interesting observation in the context of invasive

lobular carcinomas as 93.1% of these cancers are ER+. As there are no culture models of ER+ non-malignant breast epithelial cells, we evaluated the impact of increased hsa-miR-375 expression in the ER-negative (ER-) MCF10A cell line. In a 3D context, upon upregulation of hsa-miR-375, these cells formed larger colonies with disrupted tissue organization and increased proliferation These data suggest that ERα is not the only key molecule affected by hsa-miR-375 during tumourigenesis and that additional key targets, involved in three-dimensional architecture of breast epithelium, remain to be discovered.

Analysis of *hsa-miR-375* null-mice has demonstrated that hsa-miR-375 plays important roles in the development of normal pancreatic endocrine cell mass in the postnatal period, and has further demonstrated its role in the maintenance of glucose homeostasis [27,28]. Gene expression analysis of *hsa-miR-375*-null islets, from KO-mice, revealed that several hundred genes were upregulated in these cells. Using target prediction, and RT-PCR analysis, Poy *et al.* [28] validated 20 targets, which included genes with roles in the p53 pathway, MAPK signalling, apoptosis and cellular adhesion, several of which have been reported to play important roles in breast cancer.

Research in lobular cancer requires the use of cell line models. We tested the MDA-MB-134 cell line, which is considered to be of lobular origin, for the expression of hsa-miR-375 and found that it was highly elevated (data not shown), compared to that in MCF10A and MCF7 cells [45,46]. The MDA-MB-134 cells may be useful for identification of hsa-miR-375 targets. However, MCF10A cell line, a model for human mammary acinar morphogenesis recapitulates aspects of the organization of the terminal duct lobule unit (TDLU), and represents an interesting study model for analysis of the capability of candidate genes to alter mammary phenotypes and more particularly the contribution of miRNAs, as we showed it in our study.

Molecular profiling of breast lesions associated with a high-risk of subsequent breast cancer development represents a potential approach to developing strategies for reducing the burden of this disease. In this regard, women with lobular intra-epithelial neoplasia are of

interest given the increased risk of subsequent development of invasive breast cancer, which persists indefinitely after initial diagnosis [47]. Considering that LCIS lesions with similar histological appearance can have different outcomes, understanding the underlying molecular differences between lesions may help in predicting their behaviour. The identification of biomarkers in early lesions, which are predictive of the future clinical course of the disease, may help identify women at high risk of progression who may benefit from surgery, chemoprevention with a selective oestrogen receptor modulator, and/or increased monitoring and conversely may reduce the over-treatment of patients whose indolent disease is less likely to progress to an invasive carcinoma.

Our study demonstrates that retrospective analysis of archived benign and pre-invasive breast lesions, from large cohorts with extensive follow-up, has potential to help identify and develop predictors for breast lesions likely to progress to invasive disease [30,48,49].

Acknowledgements

We wish to thank Dr. Sunhee Lee for providing access to microscopy and photography for pictures of the tissues presented in this article. We thank Dr. Michael Prystowsky and Dr. Qiulu Pan for providing access to the Illumina® technology in the molecular pathology laboratories, and Michael Ronan for his technical advice and training on the Illumina® platform. For financial support, we thank Susan G. Komen for the Cure (KG100888 to PK and KG091136 to PK & OG).

Author Contributions

OL, TR, SF and NS conceived the study. SF and NS identified the suitable specimens. OL and CL isolated RNA, performed expression studies (GC provided support during miRNA profiling experiments), and qRT-PCR experiments. OL, PK and TW analyzed the expression data. AR, LS and OL performed and analyzed the in situ hybridization experiments. PAR generated the MCF10A derivatives. OG and PK designed and performed the 3D culture assays. OL and PK wrote the manuscript and all authors approved the final manuscript.

Table 1.

Case	Age	Clinical finding	Pathology	FFPE Storage (years)
Normal 1	40	Calcification	-	1
Normal 2$^{\theta}$	50	Calcification	-	2
Normal 3	19	Reduction	-	0.5
Normal 4	53	Reduction	-	0.5
Normal 5	51	Reduction	-	0.5

Case	Age	Clinical finding	LCIS Nuclear grade	Comedo Necrosis	FFPE Storage (years)
LCISa1$^{\theta}$	50	Calcification	2	Absent	2
LCISa2	54	Mastectomy	2	Absent	1
LCISa3	78	Calcification	2	Present	0.5
LCISa4	66	Mass/fibroadenoma	1	Absent	0.5
LCISa5	48	Calcification*	2	Absent	1
LCISa6	64	Mass/Phyllodes tumour	1	Absent	0.5
LCISa7	57	Nipple discharge/papilloma	1	Absent	1

Case	Age	Clinical	LCIS Nuclear	Comedo	FFPE

		finding	grade	Necrosis	Storage (years)
LCISsynch1[Ψ]	53	Calcium	3	Present	1
LCISsynch2	51	Mass	2	Absent	1
LCISsynch3	59	Calcium	2	Present	3
LCISsynch4	42	Mass	2	Absent	2
LCISsynch5	73	Mass	2	Absent	1
LCISsynch6	54	Mass	2	Absent	0.5
LCISsynch7	69	Mass	2	Absent	0.5
LCISsynch8	52	Calcium	3	Present	0.5
LCISsynch9		-----Sample not available------			

Case	Age	Clinical finding	Size (cm)	ER (%+)	PR (%+)	Axilla Lymph Nodes	FFPE storage (years)
ILCsynch1[Ψ]	53	Calcium	1.1	>95%	>95%	N0 (i+)	1
ILCsynch2	51	Mass	3.5	>95%	>95%	N0 (i+)	1
ILCsynch3	59	Calcium	2.0	N/A	N/A	N1 mi	3
ILCsynch4	42	Calcium	1.4	30%	10%	N1 mi	2
ILCsynch5	73	Mass	1.5	90%	0%	N0 (i+)	1

ILCsynch6	54	Mass	2.9	95%	95%	N0	0.5
ILCsynch7	69	Mass	1.5	100%	<5%	N0	0.5
ILCsynch8		-----Sample not available------					
ILCsynch9	74	Mass	4.5	90%	60%	N0	0.5

LEGENDS.

Figure 1. Microdissection of paraffin-embedded lobular neoplasia samples for microRNA analysis.

Representative images of specimens used in this study. Left panels: Loss of E-cadherin immunohistochemical staining was used to diagnose lobular neoplasia. Centre panels: 10 μm haematoxylin and eosin staining was used to identify regions of interest for excision from normal and neoplastic specimens. Right panels: Pathologist-identified regions of interest were microdissected from 10 μm sections for RNA purification.

Figure 2. MiRNA profiling of normal, LCIS and ILC samples reveals a cluster of microRNAs enriched in lobular neoplasia.

Euclidean hierarchical clustering of miRNAs demonstrating variable expression between normal and neoplastic samples (ANOVA, $p < 0.02$). A set of six miRNAs upregulated in normal epithelium –Hsa-miR-224, -139, -10b, -450, -140, -365; and a set of six miRNAs, hsa-miR-203, -425-5p, -183, -565, -182 and -375 enriched in the neoplastic samples.

Figure 3. Quantitative RT-PCR analysis of hsa-miR375, hsa-miR-183, and hsa-miR-182 in Lobular Neoplasia. The quantification was performed using the $\Delta\Delta C_T$ method described in the materials and methods. The coloured bar-graphs represent miRNA expression measured in fold change ($2^{(\Delta ct\ nomal\ -\Delta Ct\ LCIS\ sample)}$, by comparison with normal lobular cells (average of 5 samples (n=5)). The endogenous controls RNU44 and RNU6B (mean of Comparative threshold (Ct) between both controls) were used to normalize miRNA expression in each specimen. Insets: Box and whisker plots showing the distribution of expression levels of each miRNA between normal (n=5), LCIS alone (n=7), LCIS synchronous with ILC (n=8), and the synchronous ILC samples (n=8), plotted as fold change. The p-value represents the test for trend of expression.

Figure 4. *In situ* hybridization analysis of hsa-mir-375 expression during lobular neoplastic progression. A. Haematoxylin and eosin analysis of archived pancreas. The picture shows the presence of several Islets of Langerhans (200x, see arrows), with one of them enlarged for morphology analysis (400x). B. *In situ* hybridization detection of hsa-miR-375 in islets of Langerhans used as a positive control for the protocol used to detect hsa-miR-375 (reference). The scramble panels show a light staining of the nuclei (red nuclear stain) and the expression of hsa-miR-375 is detected specifically in islets of Langerhans (blue/purple stain), with a light purple stain in surrounding cells. C. *In situ* hybridization detection of hsa-miR-375 in normal lobular cells and lobular neoplasia. The left column displays the negative control (scramble probe) and the right column the detection of hsa-miR-375. From top to bottom, hsa-miR-375 can be detected very weakly in the nuclei of normal lobular cells and LCIS alone (LCIS alone case#2 in qRT-PCR of hsa-miR-375 in Fig. 3), see arrows in 400x panels, respectively. High expression of hsa-miR-375 can be detected in the cytoplasm of LCIS synch cells (LCIS synch case#1 in qRT-PCR of hsa-miR-375 in Fig. 3). A weaker cytoplasmic stain is visible in ILC synch cells (ILC synch case#1 in qRT-PCR of hsa-miR-375 in Fig. 3). For each individual tissue, the nucleolar U6-RNA was tested as a second positive control (data not shown).

Figure 5 hsa-mir-375 expression disrupts mammary epithelial polarity. A. Quantitative RT-PCR of hsa-miR-375 expression in LCIS synch case#1 (Fig. 3, Hsa-miR-375 graph, first bar in LCIS synch group) and MCF10A$^{hsa\text{-}miR\text{-}375}$, and their respective normal controls. B. 2D culture of MCF10A^{ctrl} (empty lentiviral vector) and MCF10A$^{hsa\text{-}mir\text{-}375}$ cells (scale bar= 200μm). Red fluorescent protein expression indicates stable infection by lentiviral vectors. C. Three-dimensional culture in Matrigel and colony size analysis (scale bar= 100μm). D. Immunofluorescence analysis of single colonies, from MCF10A^{ctrl} and MCF10A$^{hsa\text{-}miR\text{-}375}$ in 3D

cultures using Hoechst 33342 (nuclei) and α6 integrin, a marker of mammary epithelial polarity (scale bar= 50μm).

Table 1. Clinical data on archived specimens used for qRT-PCR validations. θ represents specimens obtained from the same patient. LCIS synchronously found with ILC are termed LCIS synch, and the ILC counterpart is termed ILC synch. Identical numbers between LCIS synch and ILC synch represent specimens obtained from the same patients (ex: LCIS synch1 and ILC synch1 were obtained from the same patient). Ψ represents specimens that were also analyzed on the Illumina miRNA profiling platform. The size and lymph node status were based on the original tumour. N0 describes lymph nodes without tumour cells; N0 (i+) describes lymph nodes with tumors cells with a size <0.2 mm; N1 mi describes lymph nodes with micro-metastases >0.2 mm but <2 mm.

Supplementary Figure S1. *In situ* hybridization analysis of hsa-mir-182 expression during lobular neoplastic progression. *In situ* hybridization detection of hsa-miR-182 in normal lobular cells and lobular neoplasia. From top to bottom, hsa-miR-182 can be detected in the cytoplasm of LCIS synch cells (LCIS synch case#1 in qRT-PCR of hsa-miR-375 in Fig. 3). A weaker cytoplasmic stain is visible in ILC synch cells (ILC synch case#1 in qRT-PCR of hsa-miR-375 in Fig. 3).

REFERENCES

1. Biglia N, Mariani L, Sgro L*, et al.* Increased incidence of lobular breast cancer in women treated with hormone replacement therapy: implications for diagnosis, surgical and medical treatment. *Endocr Relat Cancer* 2007; **14**: 549-567.
2. Wasif N, Maggard MA, Ko CY*, et al.* Invasive lobular vs. ductal breast cancer: a stage-matched comparison of outcomes. *Ann Surg Oncol* 2010; **17**: 1862-1869.
3. Simpson PT, Reis-Filho JS, Gale T*, et al.* Molecular evolution of breast cancer. *J Pathol* 2005; **205**: 248-254.
4. Aulmann S, Penzel R, Longerich T*, et al.* Clonality of lobular carcinoma in situ (LCIS) and metachronous invasive breast cancer. *Breast Cancer Res Treat* 2008; **107**: 331-335.
5. Hwang ES, Nyante SJ, Yi Chen Y*, et al.* Clonality of lobular carcinoma in situ and synchronous invasive lobular carcinoma. *Cancer* 2004; **100**: 2562-2572.
6. Morandi L, Marucci G, Foschini MP*, et al.* Genetic similarities and differences between lobular in situ neoplasia (LN) and invasive lobular carcinoma of the breast. *Virchows Arch* 2006; **449**: 14-23.
7. Vos CB, Cleton-Jansen AM, Berx G*, et al.* E-cadherin inactivation in lobular carcinoma in situ of the breast: an early event in tumorigenesis. *Br J Cancer* 1997; **76**: 1131-1133.
8. O'Malley FP. Lobular neoplasia: morphology, biological potential and management in core biopsies. *Mod Pathol* 2010; **23 Suppl 2**: S14-25.
9. Sullivan ME, Khan SA, Sullu Y*, et al.* Lobular carcinoma in situ variants in breast cores: potential for misdiagnosis, upgrade rates at surgical excision, and practical implications. *Arch Pathol Lab Med* 2010; **134**: 1024-1028.
10. Venkitaraman R. Lobular neoplasia of the breast. *Breast J* 2010; **16**: 519-528.
11. Mastracci TL, Tjan S, Bane AL*, et al.* E-cadherin alterations in atypical lobular hyperplasia and lobular carcinoma in situ of the breast. *Mod Pathol* 2005; **18**: 741-751.
12. Rosen PP. Microglandular adenosis. A benign lesion simulating invasive mammary carcinoma. *Am J Surg Pathol* 1983; **7**: 137-144.
13. Rakha EA, Ellis IO. Lobular breast carcinoma and its variants. *Semin Diagn Pathol*. 2010; 27:49-61.
14. Calin GA, Sevignani C, Dumitru CD*, et al.* Human microRNA genes are frequently located at fragile sites and genomic regions involved in cancers. *Proc Natl Acad Sci U S A* 2004; **101**: 2999-3004.
15. Sotiropoulou G, Pampalakis G, Lianidou E*, et al.* Emerging roles of microRNAs as molecular switches in the integrated circuit of the cancer cell. *RNA* 2009; **15**: 1443-1461.
16. Zeng Y. Principles of micro-RNA production and maturation. *Oncogene* 2006; **25**: 6156-6162.
17. Lewis BP, Burge CB, Bartel DP. Conserved seed pairing, often flanked by adenosines, indicates that thousands of human genes are microRNA targets. *Cell* 2005; **120**: 15-20.
18. Zhang B, Pan X, Cobb GP*, et al.* microRNAs as oncogenes and tumor suppressors. *Dev Biol* 2007; **302**: 1-12.
19. Heneghan HM, Miller N, Lowery AJ*, et al.* MicroRNAs as Novel Biomarkers for Breast Cancer. *J Oncol* 2009; **2009**: 950201.
20. Loudig O, Milova E, Brandwein-Gensler M*, et al.* Molecular restoration of archived transcriptional profiles by complementary-template reverse-transcription (CT-RT). *Nucleic Acids Res* 2007; **35**: e94.
21. Chen J, Lozach J, Garcia EW*, et al.* Highly sensitive and specific microRNA expression profiling using BeadArray technology. *Nucleic Acids Res* 2008; **36**: e87.
22. Jorgensen S, Baker A, Moller S*, et al.* Robust one-day in situ hybridization protocol for detection of microRNAs in paraffin samples using LNA probes. *Methods* 2010; **52**: 375-

381.
23. Debnath J, Muthuswamy SK, Brugge JS. Morphogenesis and oncogenesis of MCF-10A mammary epithelial acini grown in three-dimensional basement membrane cultures. *Methods* 2003; **30**: 256-268.
24. Selvin S. Statistical Analysis for Epidemiologic Data (2nd edn). Oxford University Press: New York. 1996; p228.
25. Neter J, Wasserman W. Applied Linear Statistical Models: Regression, Analysis of variance, and Experimental Design. Richard D. Irwin, Inc.1974; p319.
26. Li H, Kloosterman W, Fekete DM. MicroRNA-183 family members regulate sensorineural fates in the inner ear. *J Neurosci* 2010; **30**: 3254-3263.
27. Poy MN, Eliasson L, Krutzfeldt J*, et al.* A pancreatic islet-specific microRNA regulates insulin secretion. *Nature* 2004; **432**: 226-230.
28. Poy MN, Hausser J, Trajkovski M*, et al.* miR-375 maintains normal pancreatic alpha- and beta-cell mass. *Proc Natl Acad Sci U S A* 2009; **106**: 5813-5818.
29. de Souza Rocha Simonini P, Breiling A, Gupta N*, et al.* Epigenetically deregulated microRNA-375 is involved in a positive feedback loop with estrogen receptor alpha in breast cancer cells. *Cancer Res* 2010; **70**: 9175-9184.
30. Debnath J, Brugge JS. Modelling glandular epithelial cancers in three-dimensional cultures. *Nat Rev Cancer* 2005; **5**: 675-88.
31. Iorio MV, Croce CM. MicroRNAs in cancer: small molecules with a huge impact. *J Clin Oncol* 2009; **27**: 5848-5856.
32. Hannafon BN, Sebastiani P, de Las Morenas A*, et al.* Expression of microRNAs and their gene targets are dysregulated in pre-invasive breast cancer. *Breast Cancer Res* 2011; **13**: R24.
33. Guttilla IK, White BA. Coordinate regulation of FOXO1 by miR-27a, miR-96, and miR-182 in breast cancer cells. *J Biol Chem. 2009,* **284**: 23204-23216.
34. Turashvili G, Bouchal J, Baumforth K, *et al.* Novel markers for differentiation of lobular and ductal invasive breast carcinomas by laser microdissection of microarray analysis. *BMC Cancer* 2007; **7**:55.
35. Segura MF, Hanniford D, Menendez S*, et al.* Aberrant miR-182 expression promotes melanoma metastasis by repressing FOXO3 and microphthalmia-associated transcription factor. *Proc Natl Acad Sci U S A* 2009; **106**: 1814-1819.
36. Schaefer A, Jung M, Mollekopf HJ, *et al.* Diagnostic and prognostic implications of microRNA profiling in prostate cancer*. Int J Cancer* 2010; **126**:166-76.
37. Sarver AL, French AJ, Borralho PM*, et al.* Human colon cancer profiles show differential microRNA expression depending on mismatch repair status and are characteristic of undifferentiated proliferative states. *BMC Cancer* 2009; **9**: 401.
38. Sacheli R, Nguyen L, Borgs L*, et al.* Expression patterns of miR-96, miR-182 and miR-183 in the development inner ear. *Gene Expr Patterns* 2009; **9**: 364-370.
39. Ding L, Xu Y, Zhang W*, et al.* MiR-375 frequently downregulated in gastric cancer inhibits cell proliferation by targeting JAK2. *Cell Res* 2010; **20**: 784-793.
40. Tsukamoto Y, Nakada C, Noguchi T*, et al.* MicroRNA-375 is downregulated in gastric carcinomas and regulates cell survival by targeting PDK1 and 14-3-3zeta. *Cancer Res* 2010; **70**: 2339-2349.
41. Avissar M, Christensen BC, Kelsey KT*, et al.* MicroRNA expression ratio is predictive of head and neck squamous cell carcinoma. *Clin Cancer Res* 2009; **15**: 2850-2855.
42. Ladeiro Y, Couchy G, Balabaud C*, et al.* MicroRNA profiling in hepatocellular tumors is associated with clinical features and oncogene/tumor suppressor gene mutations. *Hepatology* 2008; **47**: 1955-1963.
43. Liu AM, Poon RT, Luk JM. MicroRNA-375 targets hippo-signalling effector YAP in liver cancer and inhibits tumor properties. *Biochem Biophys Res Commun* 2010; **394**:623

44. Zhang H, Mishra A, Chintagari NR*, et al.* Micro-RNA-375 inhibits lung surfactant secretion by altering cytoskeleton reorganization. *IUBMB Life* 2010; **62**: 78-83.
45. Reis-Filho JS, Simpson PT, Turner NC, et al. FGFR1 emerges as a potential therapeutic target for lobular breast carcinomas. *Clin Cancer Res* 2006; 12: 6652–62.
46. Riggins RB, Lan JP, Zhu Y, Klimach U, Zwart A, Cavalli LR, Haddad BR, Chen L, Gong T, Xuan J, Ethier SP, Clarke R. ERRgamma mediates tamoxifen resistance in novel models of invasive lobular breast cancer. *Cancer Res*. 2008 68:8908-17
47. Bodian CA, Perzin KH, Lattes R. Lobular neoplasia. Long term risk of breast cancer and relation to other factors. *Cancer* 1996; **78**: 1024-1034.
48. Silvera SA, Rohan TE. Benign proliferative epithelial disorders of the breast: a review of the epidemiologic evidence. *Breast Cancer Res Treat* 2008; **110**: 397-409.
49. Kabat GC, Jones JG, Olson N*, et al.* Risk factors for breast cancer in women biopsied for benign breast disease: a nested case-control study. *Cancer Epidemiol* 2010; **34**: 34-39.

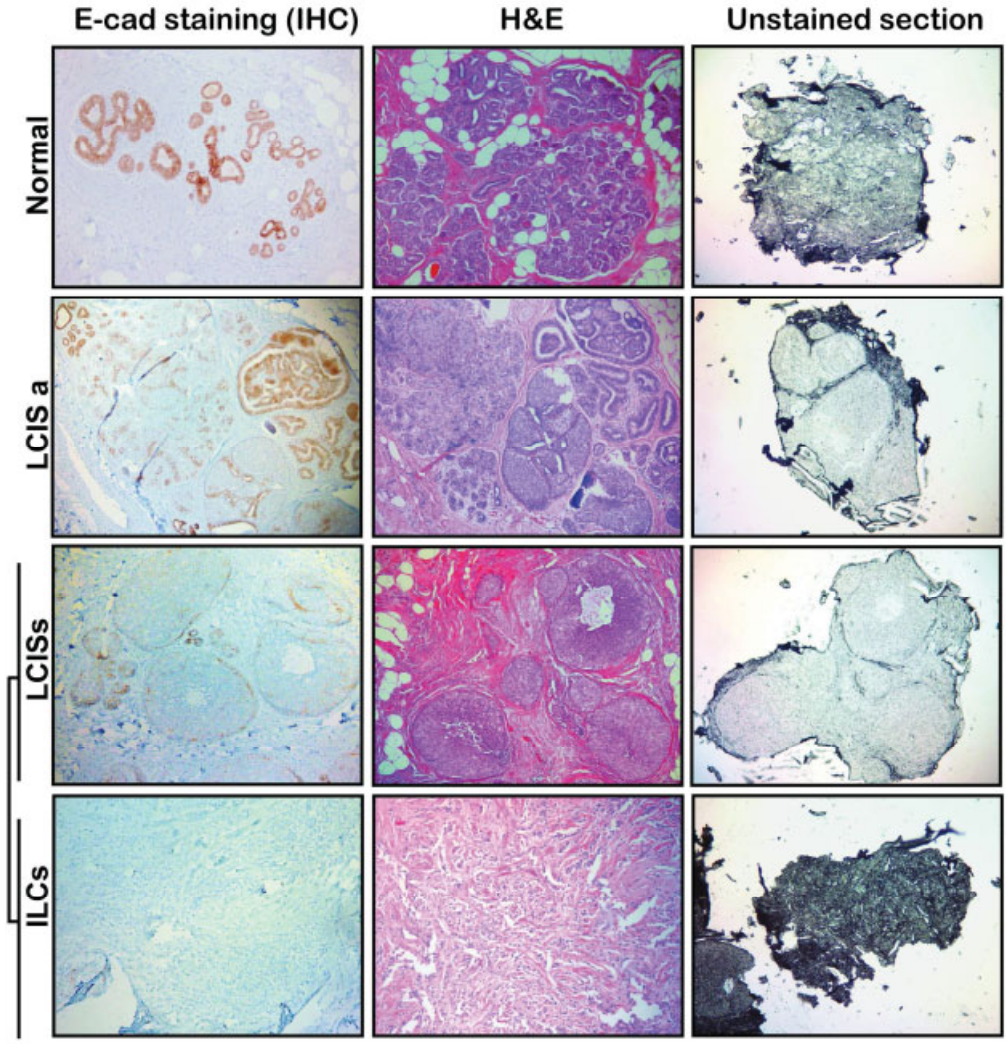
E-cad staining (IHC)
H&E
Unstained section
Normal
LCIS a
LCISs
ILCs

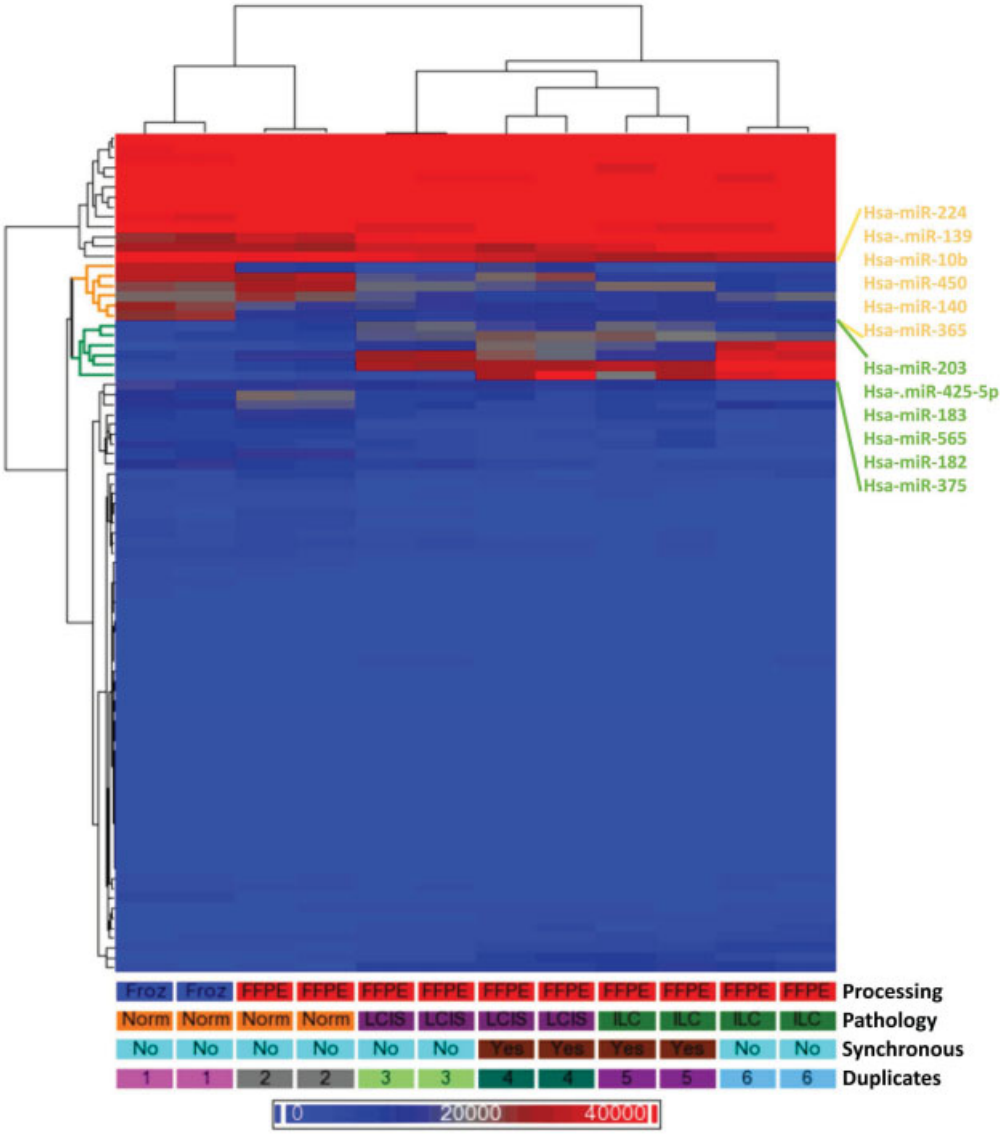
Hsa-miR-224
Hsa-.miR-139
Hsa-miR-10b
Hsa-miR-450
Hsa-miR-140
Hsa-miR-365
Hsa-miR-203
Hsa-.miR-425-5p
Hsa-miR-183
Hsa-miR-565
Hsa-miR-182
Hsa-miR-375
Froz Froz FFPE FFPE FFPE FFPE FFPE FFPE FFPE FFPE FFPE FFPE Processing
Norm Norm Norm Norm LCIS LCIS LCIS LCIS ILC ILC ILC ILC Pathology
No No No No No No Yes Yes Yes Yes No No Synchronous
1 1 2 2 3 3 4 4 5 5 6 6 Duplicates
0 20000 40000

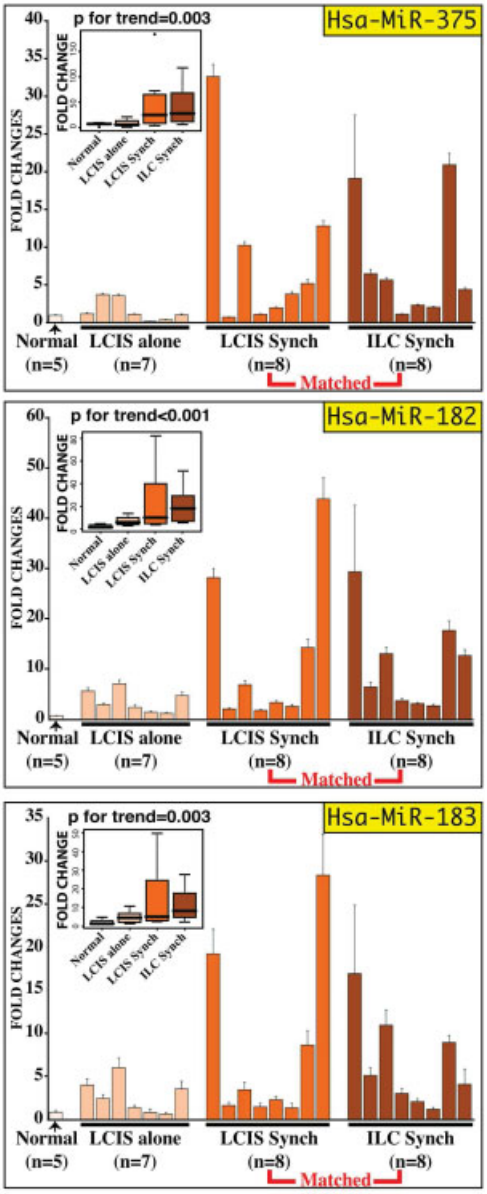
Hsa-MiR-375
p for trend=0.003
FOLD CHANGE
FOLD CHANGES
Normal
LCIS alone
LCIS Synch
ILC Synch
Normal (n=5)
LCIS alone (n=7)
LCIS Synch (n=8)
ILC Synch (n=8)
Matched
Hsa-MiR-182
p for trend<0.001
Hsa-MiR-183
p for trend=0.003

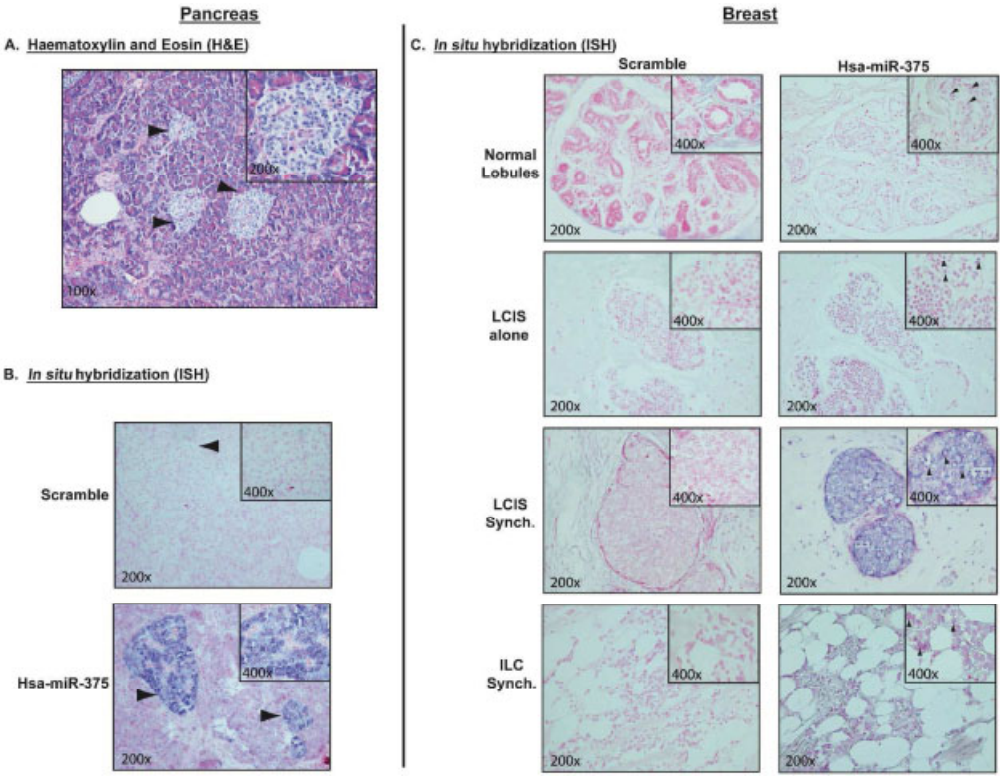
Pancreas
A. Haematoxylin and Eosin (H&E)
200x
100x
B. In situ hybridization (ISH)
Scramble
400x
200x
Hsa-miR-375
400x
200x
Breast
C. In situ hybridization (ISH)
Scramble
Hsa-miR-375
Normal Lobules
LCIS alone
LCIS Synch.
ILC Synch.
400x
200x

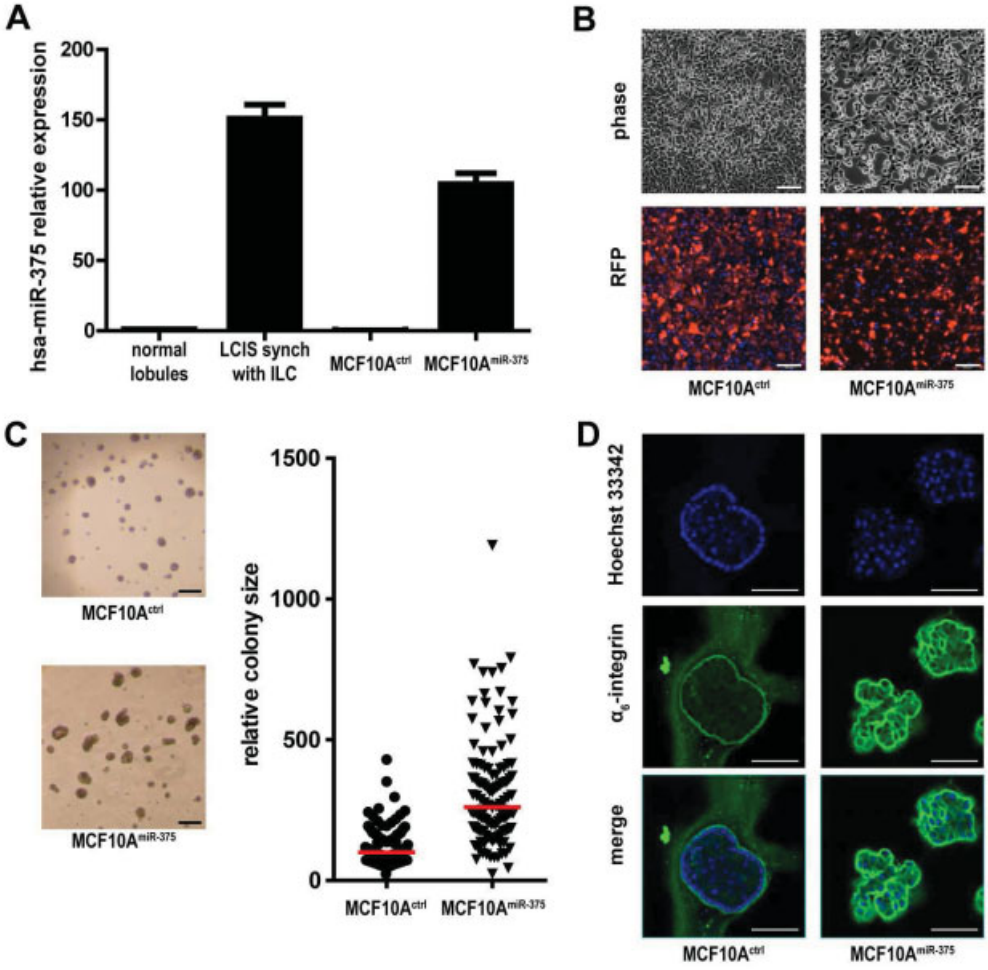
A
hsa-miR-375 relative expression
200
150
100
50
0
normal lobules
LCIS synch with ILC
MCF10Actrl
MCF10AmiR-375
B
phase
RFP
MCF10Actrl
MCF10AmiR-375
C
MCF10Actrl
MCF10AmiR-375
relative colony size
1500
1000
500
0
MCF10Actrl
MCF10AmiR-375
D
Hoechst 33342
α6-integrin
merge
MCF10Actrl
MCF10AmiR-375

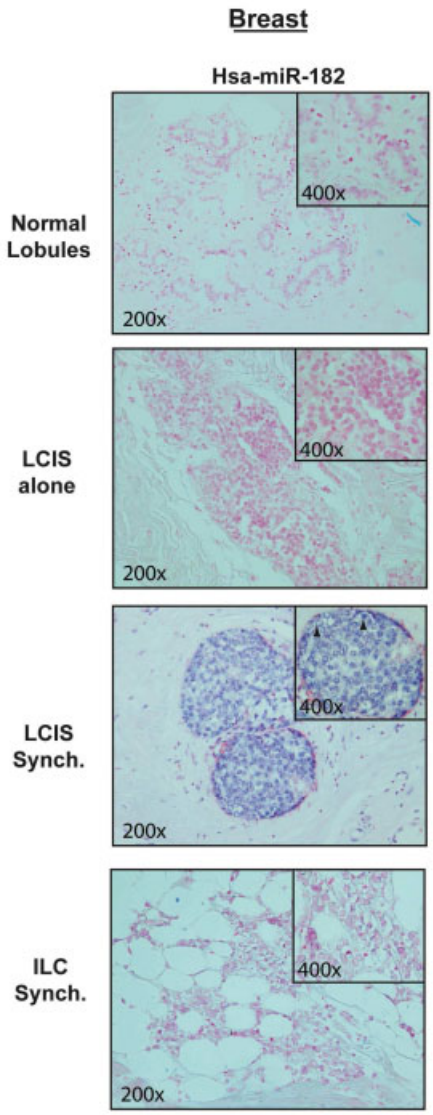

Additional Figure .

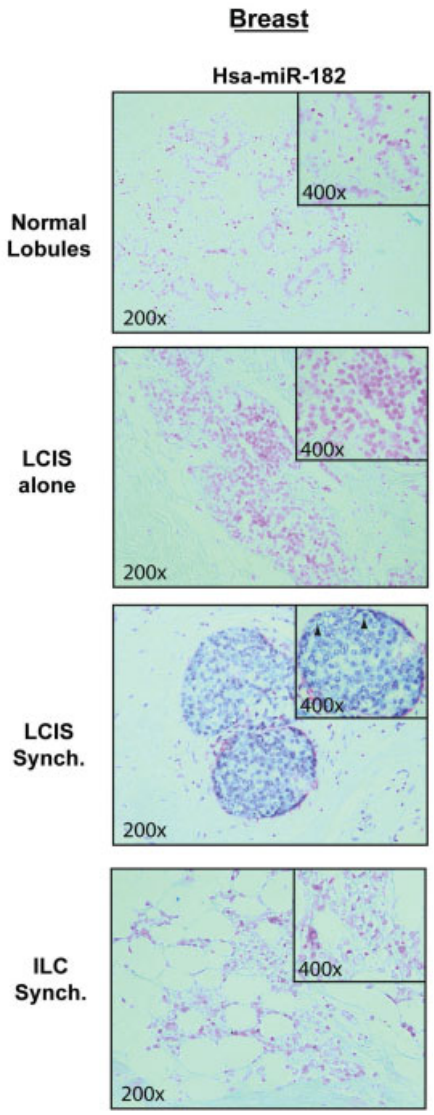

Additional Figure .